

Fluorescence Detection of a Lipid-induced Tetrameric Intermediate in Amyloid Fibril Formation by Apolipoprotein C-II^{*S}

Received for publication, May 26, 2008, and in revised form, October 7, 2008. Published, JBC Papers in Press, October 13, 2008, DOI 10.1074/jbc.M804004200

Timothy M. Ryan, Geoffrey J. Howlett¹, and Michael F. Bailey

From the Department of Biochemistry and Molecular Biology, Bio21 Molecular Science and Biotechnology Institute, University of Melbourne, Parkville, Victoria 3010, Australia

The misfolding and self-assembly of proteins into amyloid fibrils that occurs in several debilitating and age-related diseases is affected by common components of amyloid deposits, notably lipids and lipid complexes. We have examined the effect of the short-chain phospholipids, dihexanoylphosphatidylcholine (DHPC) and dihexanoylphosphatidylserine (DHPS), on amyloid fibril formation by human apolipoprotein C-II (apoC-II). Micellar DHPC and DHPS strongly inhibited apoC-II fibril formation, whereas submicellar levels of these lipids accelerated apoC-II fibril formation to a similar degree. These results indicate that the net negative charge on DHPS, compared with the neutrally charged DHPC, is not critical for either the inhibition or activation process. We also investigated the mechanism for the submicellar, lipid-induced activation of fibril formation. Emission data for fluorescently labeled apoC-II indicated that DHPC and DHPS stimulate the early formation and accumulation of oligomeric species. Sedimentation velocity and equilibrium experiments using a new fluorescence detection system identified a discrete lipid-induced tetramer formed at low apoC-II concentrations in the absence of significant fibril formation. Seeding experiments showed that this tetramer was on the fibril-forming pathway. Fluorescence resonance energy transfer experiments established that this tetramer forms rapidly and is stabilized by submicellar, but not micellar, concentrations of DHPC and DHPS. Several recent studies show that oligomeric intermediates in amyloid fibril formation are toxic. Our results indicate that lipids promote on-pathway intermediates of apoC-II fibril assembly and that the accumulation of a discrete tetrameric intermediate depends on the molecular state of the lipid.

Amyloid fibrils are formed by the self-assembly of naturally occurring proteins that misfold and aggregate into structures that share a number of common properties. The defining characteristics include increased β -structure compared with the

native form of the protein, a fibrillar cross- β -morphology, and the ability to interact with the dyes thioflavin T and Congo Red (1). The presence of specific fibrils in amyloid deposits associated with common neurodegenerative diseases, including Alzheimer and Parkinson diseases, has drawn considerable attention to the factors that affect amyloid fibril formation and the role of these fibrils in disease. Several factors within amyloid plaques exert effects on fibril formation, including metal ions, glycosaminoglycans, and proteins, such as serum amyloid P and apolipoprotein E (2). One important factor is the presence of lipids and lipid complexes, which are common components of all amyloid deposits. Fibrillogenesis by the $A\beta^2$ peptide (3), α -synuclein (4), or the islet amyloid polypeptide (5) is increased significantly by phospholipids in a manner that depends on the net charge of the phospholipid. Lipid bilayers composed of negatively charged phosphatidylserine or other anionic phospholipids accelerate amyloid fibril formation by several proteins relative to control neutral lipids (6). Micellar lipids, such as short-chain oxidized phospholipids, are present in human plasma (7). These chemically modified and truncated lipids also have the potential to affect the disease-forming properties of amyloid fibrils. Oxidized cholesterol and 4-hydroxy nonenal (8, 9) accelerate fibril formation by $A\beta$ and α -synuclein, whereas oxidized cholesterol also accelerates amyloid fibril formation by human apolipoprotein C-II (apoC-II) (10).

ApoC-II is one of several members of the plasma apolipoprotein family that form amyloid fibrils (11). ApoC-II is a normal component of very low density lipoproteins, where it plays an important physiological role as an activator of lipoprotein lipase. In the absence of lipids and under physiological conditions, apoC-II readily self-associates to form twisted ribbon-like fibrils with all of the hallmarks of amyloid (12). Immunohistochemical studies indicate the presence of apoC-II deposits in human coronary artery plaques co-localized with serum amyloid P, a widely used marker of *in vivo* amyloid (13). Fibrils formed from both apoC-II and $A\beta$ initiate early events in heart disease, including the induction of several markers of the macrophage inflammatory response (14, 15).

In the presence of high concentrations of lipid micelles, apoC-II adopts a predominantly α -helical structure (16, 17),

* This work was supported by Australian Research Council Grant DP0449510 and National Health and Medical Research Council of Australia Grant 350229. The costs of publication of this article were defrayed in part by the payment of page charges. This article must therefore be hereby marked "advertisement" in accordance with 18 U.S.C. Section 1734 solely to indicate this fact.

^S The on-line version of this article (available at <http://www.jbc.org>) contains supplemental Figs. S1–S3.

¹ To whom correspondence should be addressed. Tel.: 61-3-8344-2274; Fax: 61-3-9347-7730; E-mail: ghowlett@unimelb.edu.au.

² The abbreviations used are: $A\beta$, amyloid β ; apo, apolipoprotein; CMC, critical micelle concentration; DHPC, 1,2-dihexanoyl-*sn*-glycero-3-phosphocholine; DHPS, 1,2-dihexanoyl-*sn*-glycero-3-phosphoserine; FDS, fluorescence detection system; FRET, fluorescence resonance energy transfer; GdnHCl, guanidine hydrochloride; ThT, thioflavin T.

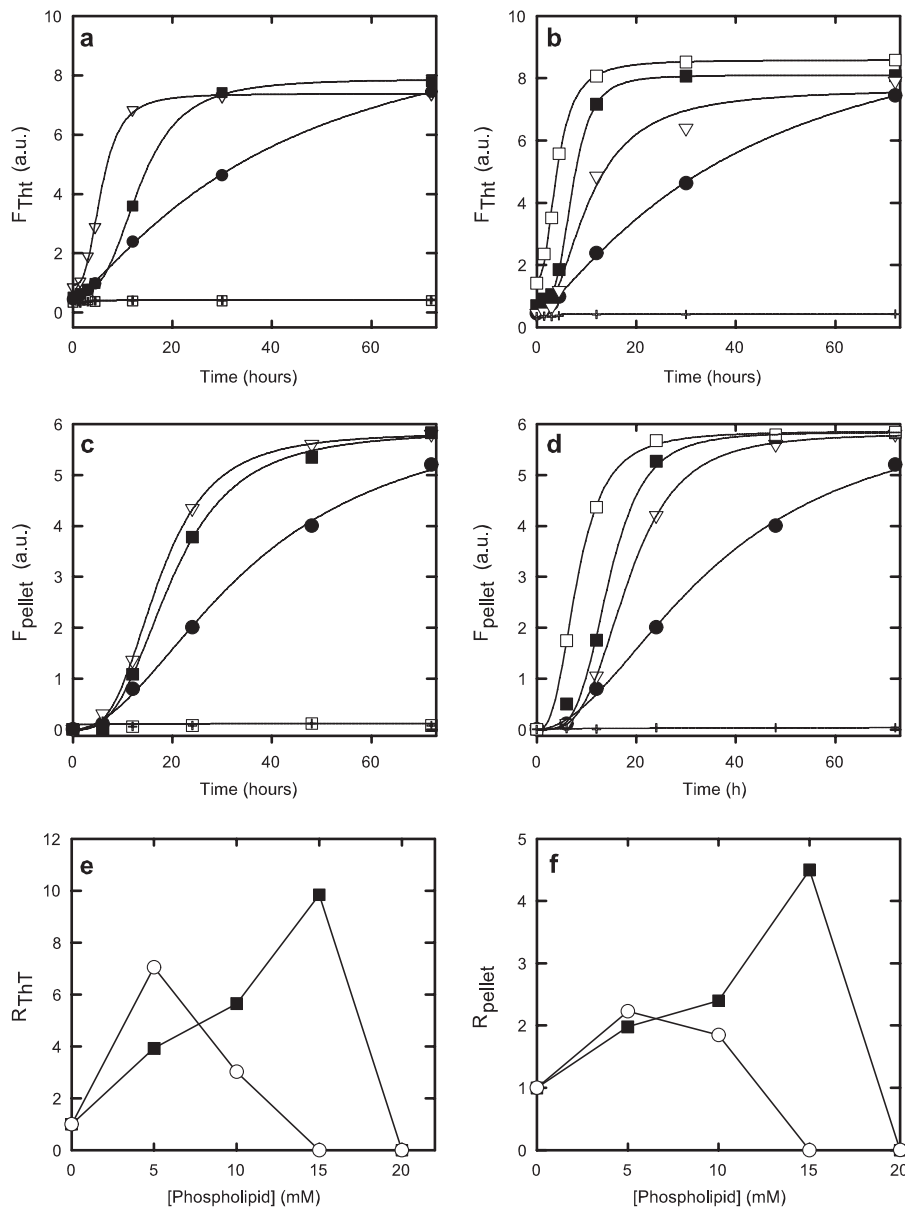


FIGURE 1. The effect of DHPC and DHPS on apoC-II fibril formation. Fibril formation was monitored by ThT fluorescence (a and b) or by the fluorescence intensity of Alexa488-labeled apoC-II in the pellet fraction after preparative ultracentrifugation (c and d). The concentrations of DHPC (a and c) and DHPS (b and d) were 0 (closed circles), 5 mM (open triangles), 10 mM (closed squares), 15 mM (open circles), and 20 mM (crosses). The rate of apoC-II fibril formation (expressed as the reciprocal of the time for half-maximal change) was calculated as a function of phospholipid concentration for DHPC (open circles) and DHPS (closed squares) for the thioflavin T reactivity data (e) and for the preparative ultracentrifuge data (f). a.u., arbitrary fluorescence units.

presumed to resemble the native state of apoC-II bound to lipoprotein particles. However, in the presence of low concentrations of lipid complexes, apoC-II slowly forms amyloid fibrils, albeit with a distinctly different rodlike morphology compared with the twisted ribbon morphology of lipid-free apoC-II fibrils (18). To investigate the role of individual lipid molecules, we explored the effects of the model short-chain phospholipid dihexanoylphosphatidylcholine (DHPC) on apoC-II amyloid fibril formation (18, 19). These studies showed that apoC-II amyloid fibril formation is accelerated by submicellar levels of DHPC but strongly inhibited by micellar DHPC (18, 19). These results indicated that individual lipid molecules play an important role in amyloid fibril self-assembly.

show that submicellar levels of DHPC and DHPS promote the rapid formation of a stable tetramer that is on the pathway for amyloid fibril formation.

EXPERIMENTAL PROCEDURES

Materials—DHPS and DHPC were obtained from Avanti Polar Lipids, Inc. (Alabaster, AL), and Alexa488 C₅ maleimide and Alexa594 C₅ maleimide were obtained from Invitrogen. ApoC-II was expressed and purified as described previously (12). Purified apoC-II stocks were stored in 5 M guanidine hydrochloride (GdnHCl), 10 mM Tris·HCl, pH 8.0, at a concentration of ~45 mg/ml. ApoC-II_{S61C} was provided by Dr. Chi Pham (University of Melbourne). ApoC-II_{S61C} was conjugated

The initial aim of our study was to compare the activating effects of submicellar concentrations of the neutral phospholipid, DHPC, with the structurally related negatively charged phospholipid, dihexanoylphosphatidylserine (DHPS).

Interest in the structural details of intermediates involved in amyloid fibril formation arises from the postulate that small oligomeric species mediate the disease-related effects of amyloid fibrils (20–22). However, a major difficulty in defining these species is the low steady-state concentrations of intermediates in amyloid fibril-forming pathways. Studies on the kinetics of fibril formation generally indicate a distinct lag phase attributed to a slow nucleation event that provides the seed for subsequent fibril elongation. Our recent studies of the size distribution of apoC-II fibrils and concentration dependence of apoC-II fibril formation led to the development of a reversible kinetic model involving an initial nucleation event followed by elongation, coupled with fibril breaking and joining (23). Within the limits of our analysis, the size of the amyloidogenic nucleus involved in apoC-II amyloid fibril formation could not be unequivocally assigned. The recent development of a new fluorescence detection system for the analytical ultracentrifuge (24) afforded a unique opportunity to explore the existence of stable populations of oligomeric intermediates formed at low apoC-II concentrations where fibril formation does not occur. Using this approach, in conjunction with fluorescence spectroscopy, we

Effects of Phospholipids on Amyloid Fibril Formation

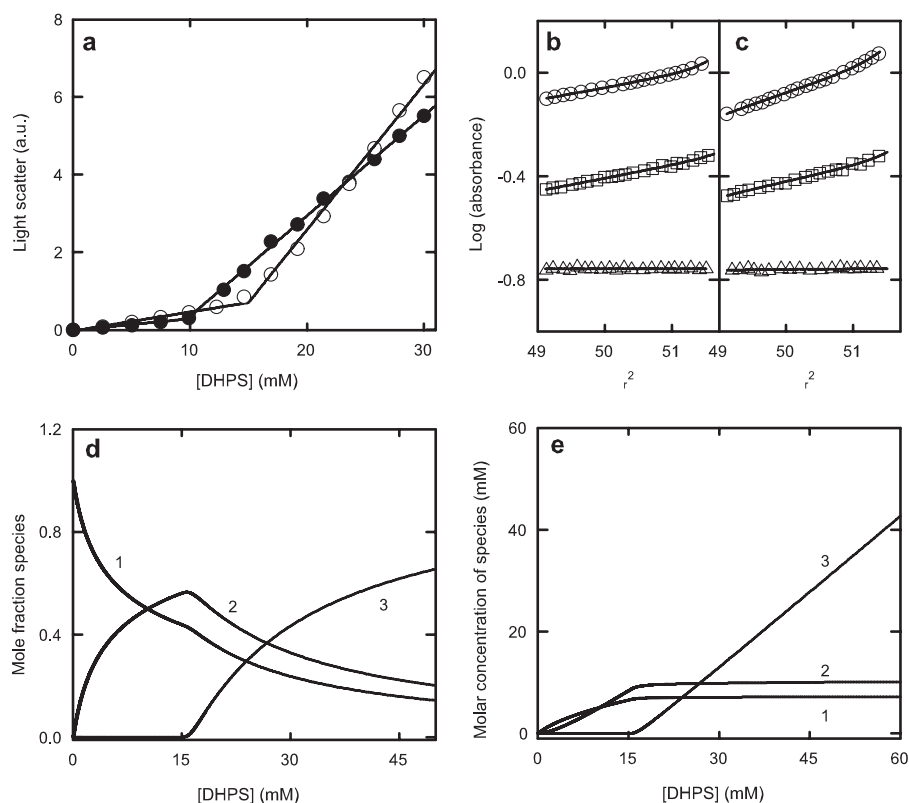


FIGURE 2. Light scattering and sedimentation analysis of micelle formation by DHPC and DHPS. *a*, intensity of scattered light at 400 nm as a function of added DHPC (closed circles) or DHPS (open circles). *b* and *c*, sedimentation equilibrium data, plotted as log (absorbance 230 nm) versus radius (r) squared, for 2.5 mM (open triangles), 12 mM (open squares), and 24 mM (open circles) DHPS and obtained at 20 °C and 24,000 (*b*) and 38,000 rpm (*c*) ($46,500 \times g$ and $116,000 \times g$, respectively). The data were fitted using Sedphat (28), assuming a monomer-dimer-micelle equilibrium (solid lines) yielding association constants of $k_{1,2} = 72.96 \pm 3.8 \text{ M}^{-1}$ and $k_{2,n} = 1.24 \times 10^{16} \pm 1.35 \times 10^3 \text{ M}^{-36}$ ($n = 37$). These equilibrium constants were used to calculate the molar concentrations of monomer (curve 1), dimer (curve 2), and micelle (curve 3) in *d* and the molar fractions of the species (*e*). *a.u.*, arbitrary light emission units.

with Alexa dyes, as described by the product manual. Briefly, the sample was incubated with a 3-fold molar excess of Alexa488 or Alexa594 C₅ maleimide for 90 min at room temperature. Free Alexa maleimide was removed by gel filtration with a G25 Sephadex column (GE Healthcare). The labeling efficiency was determined spectrophotometrically, assuming molar extinction coefficients of Alexa488 at 495 nm of $71,000 \text{ M}^{-1} \text{ cm}^{-1}$, Alexa594 at 590 nm of $95,000 \text{ M}^{-1} \text{ cm}^{-1}$, and apoC-II at 280 nm of $11,000 \text{ M}^{-1} \text{ cm}^{-1}$. Labeling efficiencies were typically >95%, and labeled samples were stored as a 1.8 mg/ml stock at $-20 \text{ }^\circ\text{C}$ in 5 M GdnHCl. Aliquots of phospholipid in chloroform (2 mg/ml) were evaporated under a gentle stream of nitrogen gas and used to prepare aqueous solutions by the addition of the required buffer. The critical micelle concentration (CMC) of the unlabeled short-chain phospholipids was determined using Rayleigh light scattering measurements, as described previously (25).

ApoC-II Amyloid Fibril Formation—ApoC-II was refolded by dilution to 0.3 mg/ml from a stock solution into refolding buffer (100 mM sodium phosphate, 0.1% sodium azide, pH 7.4). ApoC-II amyloid fibril formation was monitored by taking sample aliquots, in triplicate, at selected time points and determining the change in thioflavin T (ThT; $10 \mu\text{M}$) fluorescence intensity measured in an fmax fluorescence plate reader

(Molecular Devices, Sunnyvale, CA) equipped with 444-nm excitation and 485-nm emission filters. A centrifuge-based assay was also used to monitor the rate of Alexa488 apoC-II assembly into amyloid fibrils. Labeled apoC-II was refolded in refolding buffer, and residual GdnHCl was removed using an NAP5 desalting column (GE Healthcare). At intervals, 100- μl aliquots were centrifuged for 30 min at 100,000 rpm ($350,000 \times g$) in an OptimaMax centrifuge using a TL-100.1 rotor (Beckman Coulter Instruments, Inc., Fullerton, CA). The pellet was washed with refolding buffer and dissolved in 100 μl of 5 M GdnHCl. The emission spectrum of the sample was recorded on a SPEX Fluorolog- τ 2 spectrofluorimeter (Horiba Jobin Yvon, Edison, NJ) using an excitation wavelength of 495 nm and collecting the emission over the range 495–700 nm using a 495-nm long pass filter.

Circular Dichroism Spectroscopy—CD measurements were made using an Aviv model 62 DS CD spectrometer (Aviv Associates Inc., Lakewood, NJ) at 25 °C with a 1-mm path length quartz cuvette, a spectral bandwidth of 1 nm, a signal averaging time of 2 s, and a data interval of

0.5 nm. The spectra presented are the average of two duplicates and corrected using a reference solution lacking apoC-II. Data were analyzed using CDPro (26).

Time Course of Alexa488-labeled ApoC-II Fluorescence—Refolded Alexa488-labeled apoC-II in the presence or absence of lipids was transferred to a 96-well fluorescence plate, and 30 μl of mineral oil was layered on top of each sample to reduce evaporation. The fluorescence emission and anisotropy of the samples was measured using a Paradigm fluorescence plate reader (Beckman Coulter Instruments) equipped with 485-nm excitation and 538-nm emission filters. Control experiments showed that oil overlay did not affect the lipid-induced fluorescence changes of the Alexa488-labeled apoC-II.

Sedimentation Analysis—Sedimentation experiments were conducted using an XL-A analytical ultracentrifuge (Beckman Coulter Instruments), an An-Ti60 rotor, and double-sector 12-mm path length cells containing sapphire windows and charcoal-filled epon centerpieces. A fluorescence detection system (FDS; Aviv Biomedical) was used to monitor the fluorescence of labeled apoC-II derivatives. The FDS uses a 488-nm frequency doubled 13-milliwatt solid state laser and confocal optics to excite a small spot in the solution column. The emission is directed through a 505-nm cut-off filter and into a photomultiplier tube for signal digitization (24). Sedimentation

velocity data for Alexa488-labeled apoC-II were obtained at 20 °C using a rotor speed of 50,000 rpm (200,000 $\times g$). Fluorescence data were collected at 1-min intervals from 6 to 7.25 cm with the excitation laser focused at a spot 20 μm in diameter, 31 μm below the surface of the sapphire window. Sedimentation equilibrium data were collected using the FDS attachment for samples of Alexa488-labeled apoC-II and rotor speeds of 26,000 and 38,000 rpm (54,500 $\times g$ and 116,000 $\times g$, respectively). Sedimentation velocity data were analyzed using the $c(s)$ program SEDFIT 9.4 (27) and maximum entropy regularization to convert the experimental data into a continuous size distribution. Sedimentation equilibrium data were analyzed assuming a noninteracting species model using the SEDPHAT program (28).

Fluorescence Resonance Energy Transfer—Emission spectra of samples, in triplicate, containing a 1:4 mixture of Alexa488- and Alexa594-labeled apoC-II in the presence of a range of DHPS concentrations were recorded on an SPEX Fluorolog- τ 2 spectrofluorimeter using an excitation wavelength of 480 nm (2-nm bandwidth) and collecting the emission intensity over the range 495–750 nm with a 495-nm long pass filter.

Seeding of Amyloid Fibril Formation—ApoC-II (50 $\mu\text{g}/\text{ml}$) was incubated in refolding buffer in the presence or absence of 10 mM DHPS. At 15-min intervals, 100 μl of these solutions were withdrawn and diluted with buffer (1.9 ml) containing freshly refolded apoC-II (final concentration 0.2 mg/ml), and the rate of fibril formation was monitored using the ThT assay.

RESULTS

The Effect of DHPC and DHPS on ApoC-II Fibril Formation—The time course for apoC-II fibril formation in the presence of various concentrations of DHPC and DHPS was monitored by ThT fluorescence (Fig. 1). In the absence of added phospholipid, ThT fluorescence increased with a small but discernable lag phase, as previously reported (23). The addition of submicellar DHPC (5 and 10 mM) increased the rate of fibril formation, whereas micellar DHPC inhibited fibril formation, consistent with previous studies (18, 19). The addition of the negatively charged derivative, DHPS, gave similar results; DHPS at concentrations of 5 and 10 mM accelerated the rates of apoC-II fibril formation, whereas 20 mM DHPS inhibited fibril formation. In view of the potential for the negative charge on DHPS to affect ThT fluorescence measurements, we also conducted a centrifugal pelleting assay using Alexa488-labeled apoC-II. The results show similar trends with low concentrations of DHPC and DHPS accelerating fibril formation and high concentrations causing inhibition. Electron microscopy confirmed that the morphologies of Alexa488-labeled apoC-II fibrils and fibrils formed in the presence of DHPS were similar to unlabeled apoC-II fibrils (supplemental material).

The kinetic data for fibril formation were fitted empirically to a three-parameter Hill equation (solid lines) to obtain estimates for the time to reach half-maximal fibril formation (t_{50}), as shown previously (29). The rates of fibril formation, expressed as the reciprocal of t_{50} , are plotted in Fig. 1. The ThT data show maximum rate increases for DHPC and DHPS of ~ 7 - and 10-fold, respectively, whereas the data for the pelleting assay show corresponding increases of 2.5- and 4.5-fold. Comparison

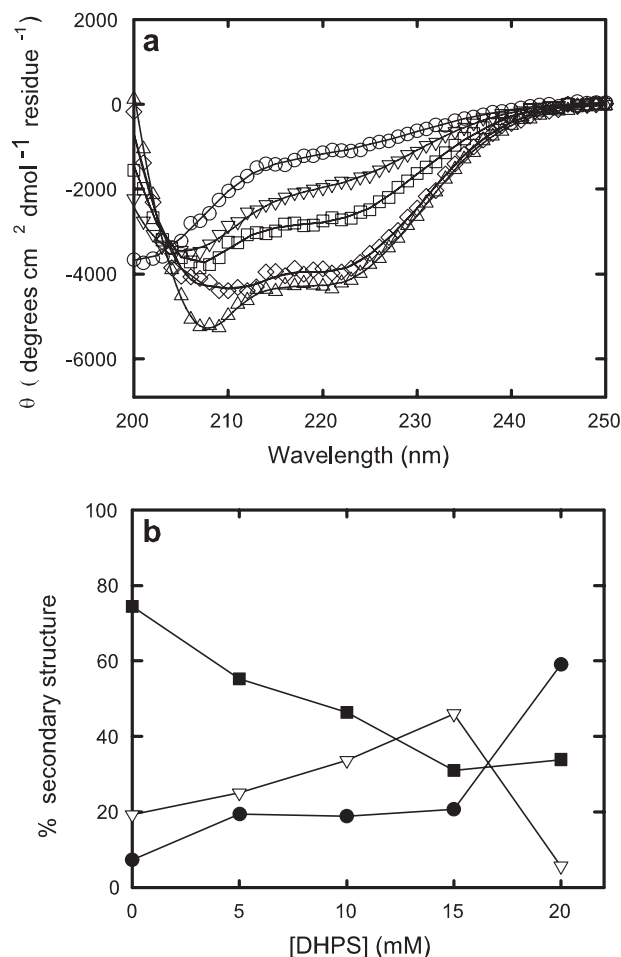


FIGURE 3. **CD spectra of freshly prepared apoC-II.** *a*, CD spectra of apoC-II (50 $\mu\text{g}/\text{ml}$) in the absence of phospholipid (open circles) and presence of 5 mM (squares), 10 mM (triangles), 15 mM (diamonds), and 20 mM (inverted triangles) DHPS. *b*, the data in *a* were fitted to obtain the relative proportions of α (closed circles), β (inverted triangles), and random (closed squares) structure.

of the results for DHPC and DHPS indicates that the negative charge on DHPS, compared with DHPC, does not exert a major effect on the rate of apoC-II fibril formation.

The Micellar State of DHPC and DHPS—To further interpret the DHPC and DHPS-mediated effects, we examined the micellar state of these lipids. Critical micelle concentrations of DHPC and DHPS were estimated using light scattering measurements. Two distinct linear phases in light scattering for the two phospholipids were observed (Fig. 2). The breakpoints in the two phases provide estimates of 10.1 and 15.2 mM for the CMCs of DHPC and DHPS, respectively. The value obtained for DHPC is in good agreement with previous estimates obtained under similar conditions (30, 31). The increase in the CMC for DHPS compared with DHPC is consistent with the higher concentrations of DHPS required to attain the maximum increase in the rate of apoC-II fibril formation (Fig. 1).

NMR spectroscopy, sedimentation equilibrium, and microcalorimetry data indicate that DHPC micelle formation proceeds via the formation of a dimeric intermediate (30, 32). Sedimentation equilibrium experiments were carried out to provide a more complete analysis of the micellar state of DHPS (Fig. 2). The results obtained for DHPS were incompatible with

Effects of Phospholipids on Amyloid Fibril Formation

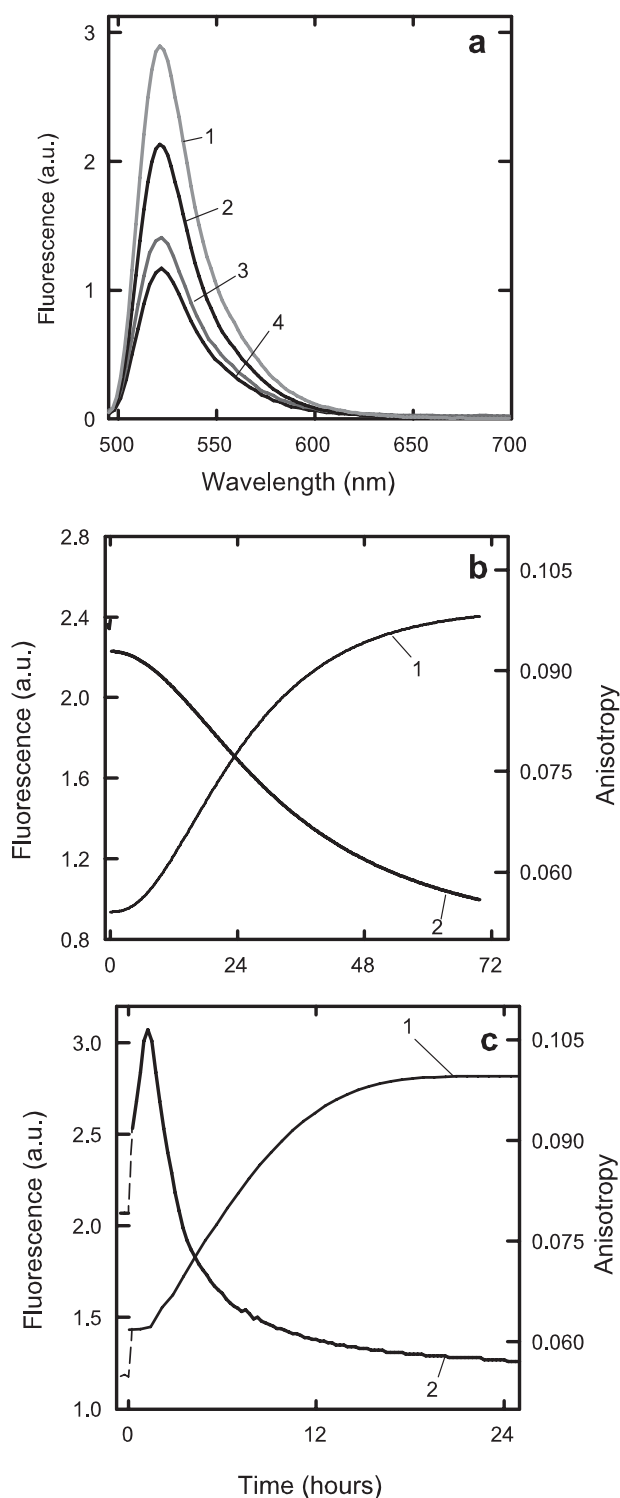


FIGURE 4. Fluorescence spectroscopy of Alexa488-labeled apoC-II. *a*, fluorescence spectra of freshly prepared Alexa488-labeled apoC-II (50 $\mu\text{g/ml}$; excitation at 495 nm) in the absence of lipid (curve 2) and in the presence of 10 mM DHPS (curve 1) and of preformed, fibrillar Alexa488-labeled apoC-II (formed at 0.3 mg/ml and diluted to 50 $\mu\text{g/ml}$) in the absence (curve 4) and presence (curve 3) of 10 mM DHPS. *b*, fibril formation by Alexa488-labeled apoC-II (0.3 mg/ml) was monitored by the fluorescence intensity (curve 2) and anisotropy (curve 1). *c*, as for *b* but in the presence of 10 mM DHPS. *a.u.*, arbitrary fluorescence units.

a simple monomer-micelle equilibrium but were consistent with a monomer-dimer-micelle equilibrium. Global fits using this model (*solid lines*), with assigned values for the molecular

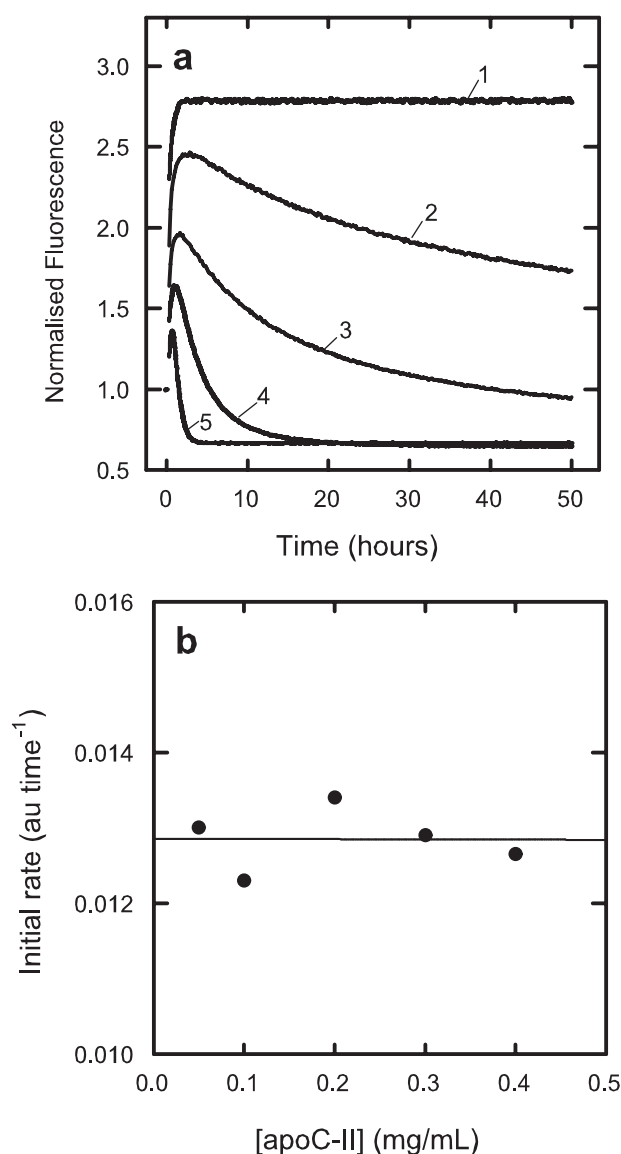


FIGURE 5. Time dependence of the fluorescence emission of Alexa488-labeled apoC-II in the presence of 10 mM DHPS (485-nm excitation and 538-nm emission filters). *a*, the concentrations of Alexa488 apoC-II were 0.05, 0.1, 0.2, 0.3, and 0.4 mg/ml (for curves 1–5, respectively). The data are normalized to the initial fluorescence of the solution. *b*, the initial rate of change in fluorescence emission (in arbitrary fluorescence units (*au*) per time) as a function of Alexa-labeled apoC-II concentration.

weights of the DHPS monomer and dimer, yielded best fit values for the molecular mass of the DHPS micelle (17,700 Da) and the equilibrium constants for the interactions. This allowed the concentration of the three species to be calculated as a function of DHPS concentration (Fig. 2). The results confirm a CMC for DHPS of ~ 15 mM and a concentration-dependent increase in the dimeric intermediate over the 0–15 mM range. These results may be compared with those reported for DHPC, where the dimer concentration increases over the 0–10 mM range and the CMC is ~ 10 mM (30). These data closely follow the activation profiles for DHPC and DHPS on apoC-II fibril formation.

Circular Dichroism of ApoC-II—The effect of DHPC and DHPS on the secondary structure of apoC-II was examined by CD spectroscopy. These experiments were carried out using freshly refolded apoC-II (50 $\mu\text{g/ml}$) under conditions where

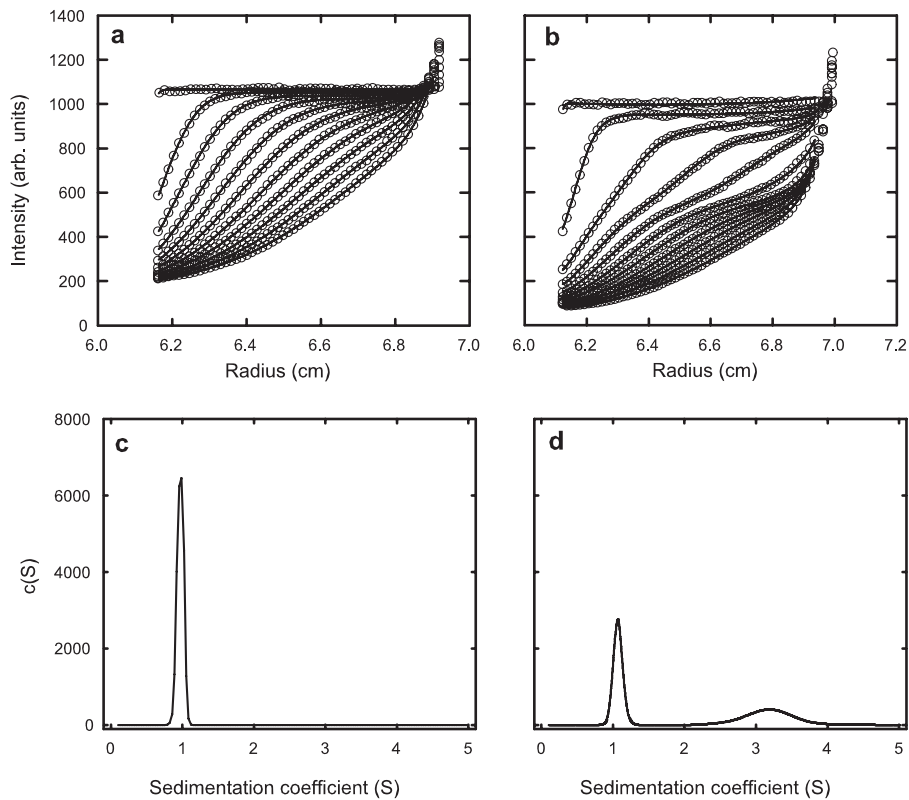


FIGURE 6. Sedimentation velocity data for freshly prepared Alexa488-labeled apoC-II (50 $\mu\text{g}/\text{ml}$) obtained using fluorescence detection in the analytical ultracentrifuge. Shown are freshly prepared Alexa488-labeled apoC-II alone (a) and in the presence of 10 mM DHPS (b). The data were obtained using an angular velocity of 50,000 rpm ($200,000 \times g$) and time intervals of 10 min. The solid lines through the data in a and b were obtained by fitting the data to a continuous size distribution $c(s)$ model (41), yielding the distributions in c and d, respectively.

fibril formation is negligible. DHPS increased the negative ellipticities in the 205–240 nm region, indicative of an increase in secondary structure (Fig. 3). Analysis of the data, assuming the presence of α , β , and random structure, allowed the proportions of these elements to be determined as a function of DHPS concentration. Submicellar concentrations of DHPS increased the proportion of β -structure relative to α -structure, whereas micellar concentrations of DHPS promote increased α -structure. Similar changes in apoC-II secondary structure were also observed with DHPC with an increase in the proportion of β -structure over the concentration range 0–10 mM DHPC and subsequent increase in α -structure in the presence of micellar DHPC (results not shown). The increase in α -structure induced by micellar DHPC and DHPS is consistent with the predominantly α -helical structures determined for apoC-II in lipid micelles (16, 17).

Fluorescence Spectroscopy of Alexa488-labeled ApoC-II—A continuous, fluorescence-based assay using Alexa488-labeled apoC-II was developed to provide more detailed information on the kinetics of fibril formation. Fluorescence spectra for both freshly refolded and fibrillar Alexa488-labeled apoC-II show characteristic maxima at 520 nm (Fig. 4). The fluorescence intensity of freshly refolded apoC-II is ~ 2 -fold higher than the fibrillar form, demonstrating that the Alexa488 probe is quenched upon fibril formation. The addition of 10 mM DHPS to freshly refolded and fibrillar Alexa488-labeled apoC-II resulted in an increase in the 520-nm emission. DHPC

also increased the fluorescence intensity of freshly refolded and fibrillar Alexa488-labeled apoC-II (supplemental material). Control experiments showed that DHPS and DHPC had no effect on the fluorescence intensity of free Alexa488 dye. The sensitivity of Alexa488-labeled apoC-II fluorescence to fibril formation provided a convenient and continuous assay for fibril formation.

Time-dependent changes in Alexa488-labeled apoC-II fluorescence emission and anisotropy under fibril-forming conditions (0.3 mg/ml) were monitored in the absence and presence of DHPS (Fig. 4). In the absence of phospholipid, there was a significant decrease in fluorescence intensity and a coincident increase in fluorescence anisotropy corresponding to fibril formation. In contrast, the time-dependent changes in fluorescence emission for Alexa488-labeled apoC-II in the presence of 10 mM DHPS showed complex kinetics with an initial very rapid increase in fluorescence intensity within the dead time of the measurement. This

fluorescence increase was accompanied by a similar rapid increase in fluorescence anisotropy (dotted lines). These immediate rapid changes were followed by a time-dependent biphasic response. This involved an increase in intensity over a period of 1–2 h with no significant change in anisotropy, followed by a dominant decrease in fluorescence intensity and increase in anisotropy, corresponding to fibril formation. The complex fluorescence kinetics observed under these conditions indicated the accumulation of lipid-induced intermediates.

The nature of the lipid-induced intermediate(s) was examined by determining the biphasic fluorescence profile as a function of Alexa488-labeled apoC-II concentration in the presence of 10 mM DHPS (Fig. 5). Over the concentration range of 50–400 $\mu\text{g}/\text{ml}$ apoC-II, all samples showed an initial increase in fluorescence intensity. Samples with apoC-II concentrations of $>100 \mu\text{g}/\text{ml}$ showed a subsequent decrease attributable to fibril formation, whereas, for the 50 $\mu\text{g}/\text{ml}$ sample, the initial increase in fluorescence intensity reached a plateau value with no subsequent decrease, consistent with the observation that fibrils are not formed at this concentration. A similar concentration dependence of Alexa488-labeled apoC-II fluorescence emission was also observed with 5 mM DHPC, showing biphasic responses at apoC-II concentrations of $>100 \mu\text{g}/\text{ml}$ and a plateau value obtained at 50 $\mu\text{g}/\text{ml}$ (supplemental material). Analysis of the increase in fluorescence intensity of Alexa488-labeled apoC-II concentration in the presence of 10 mM DHPS

Effects of Phospholipids on Amyloid Fibril Formation

over the first 1 h showed that the initial rate of change was independent of apoC-II concentration (Fig. 5).

Sedimentation Velocity Analysis—The data in Figs. 4 and 5 provide evidence for a stable, lipid-induced species that forms at 50 $\mu\text{g/ml}$ Alexa488-labeled apoC-II in the absence of significant fibril formation. This suggested that the molecular state of this species would be amenable to sedimentation velocity analysis using the new high sensitivity FDS for the analytical ultracentrifuge. Fluorescence intensity scans obtained over time, during sedimentation of Alexa488-labeled apoC-II alone (50 $\mu\text{g/ml}$) and in the presence of 10 mM DHPS, are presented in Fig. 6. A single, major sedimenting boundary was observed for apoC-II alone with an additional boundary evident in the presence of DHPS. The radial scans were analyzed assuming a $c(s)$ continuous distribution of sedimentation coefficients yielding the distributions shown (Fig. 6). The results for Alexa488-labeled apoC-II alone indicate a single species with a modal sedimentation coefficient of 1 S, whereas the data in the presence of DHPS indicate two major species with modal sedimentation coefficients of 1.1 and 3.2 S. Sedimentation velocity measurements using absorbance optics (230 nm) for unlabeled apoC-II alone (50 $\mu\text{g/ml}$) and in the presence of 10 mM DHPS gave similar $c(s)$ distributions; however, the data were of poorer quality, with a low signal/noise ratio. Sedimentation velocity analysis showed that submicellar concentrations of DHPC (5 mM) and the longer chain phospholipid, 1-dodecyl-2-hydroxy-*sn*-glycero-3-phosphocholine (100 μM), also promoted the formation of a discrete faster sedimenting species (supplemental material).

Sedimentation velocity experiments using the FDS were conducted with Alexa488-labeled apoC-II over a range of DHPS concentrations, yielding the $c(s)$ distributions shown in Fig. 7. The results show three major populations with apparent sedimentation coefficients of 0.9–1.1 S (population 1), 2.2–2.6 S (population 2), and 3.0–3.5 S (population 3). As the concentration of DHPS increases, population 1 gradually diminishes, whereas populations 2 and 3 increase. Calculation of the areas under the distributions for each population showed that populations 2 and 3 are favored by micellar and submicellar DHPS, respectively. A simple interpretation of this finding is that population 2 corresponds to a submicellar DHPS-induced, oligomeric apoC-II species, whereas population 3 corresponds to a micellar bound apoC-II species.

Sedimentation Equilibrium Analysis—An assumption in $c(s)$ analysis of sedimentation velocity data is that the species are not interacting on the time scale of the experiment. An indication that reversible interactions may be occurring in this system is suggested by the variation in the sedimentation coefficients for populations 2 and 3 at different DHPS concentrations (Fig. 7). Another limitation with sedimentation velocity studies is that the analysis of sedimentation coefficients to obtain molecular weight values requires assumptions concerning molecular shape. We therefore extended our studies to sedimentation equilibrium analysis using fluorescence detection. Sedimentation equilibrium data obtained over a range of DHPS concentrations, at two different rotor speeds and in the presence of either H_2O - or D_2O -containing buffers, were analyzed globally, assuming three species, as suggested by the sedimentation

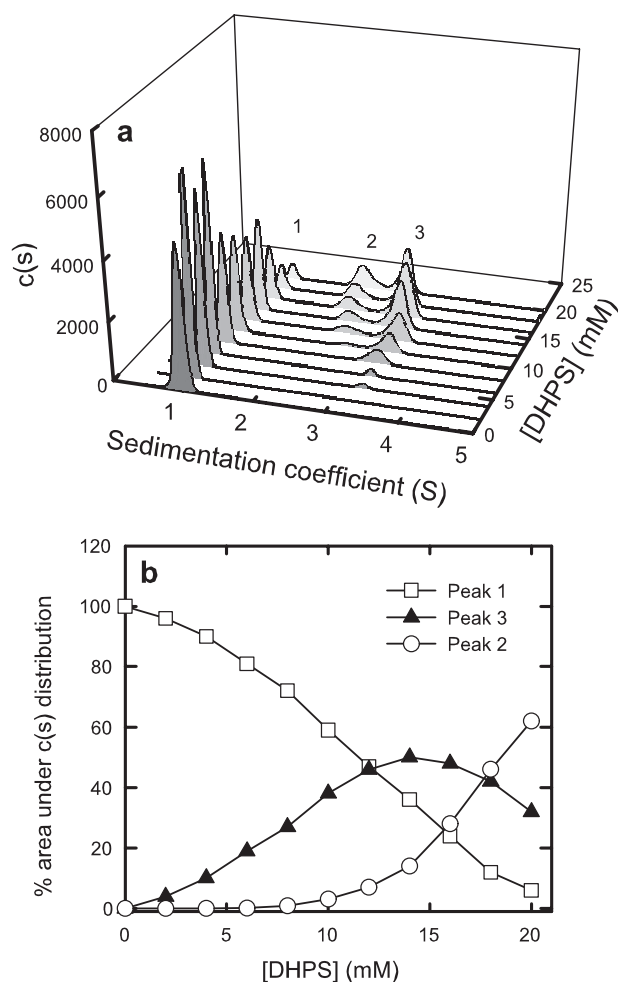


FIGURE 7. Sedimentation velocity analysis of Alexa488-labeled apoC-II obtained using fluorescence detection in the analytical ultracentrifuge. *a*, continuous size distributions, $c(s)$, for freshly prepared Alexa488-labeled apoC-II as a function of DHPS concentration. *b*, the relative areas under the peaks labeled 1, 2, and 3 in *a* as a function of DHPS concentration.

velocity data (Fig. 7). Representative sedimentation equilibrium data are presented in Fig. 8, where the *solid lines* indicate the quality of the global fits. The complete analysis, summarized in Table 1, allowed the partial specific volumes and molecular weights of the three species to be determined. The partial specific volume obtained for species 1 was close to that calculated for apoC-II alone (12). The data for species 2 indicated a predominantly lipid-free apoC-II species with a molecular weight corresponding to a tetramer, whereas the values of the partial specific volume and molecular weight for species 3 are consistent with a single molecule of apoC-II associated with a DHPS micelle (micelle M_r , 17,700). Similar sedimentation equilibrium experiments using fluorescence detection were also performed using Alexa488-labeled apoC-II over a range of DHPC concentrations. Global analysis of the data indicates that DHPC also induced the formation of an apoC-II tetramer and an apoC-II-micelle complex (Table 1). The results of the global fitting allowed the proportion of species 1, 2, and 3 to be calculated as a function of DHPC and DHPS concentration (Fig. 8). This analysis shows that the tetrameric species (species 2) is favored by submicellar lipid, whereas the micellar species (species 3) predominates at micellar lipid concentrations.

Fluorescence Resonance Transfer Analysis of ApoC-II Tetramer Formation—Our sedimentation analysis established the existence of a stable, lipid-induced tetramer that forms at low concentrations of apoC-II. To explore the formation of this tetramer at earlier time points, a fluorescence resonance energy transfer (FRET) assay was developed using Alexa488- and Alexa594-labeled apoC-II as a donor-acceptor pair. Fluorescence emission spectra (excitation 480 nm) for separate solutions of Alexa488-labeled apoC-II (50 $\mu\text{g}/\text{ml}$) and Alexa594-labeled apoC-II (50 $\mu\text{g}/\text{ml}$) exhibited characteristic maxima at 520 and 617 nm, respectively (not shown). Emission spectra for a 1:4 mixture of these solutions acquired 5 min after refolding in the absence of lipid and in the presence of 10 mM DHPS are

shown in Fig. 9. The spectrum obtained for the lipid-free mixture is equivalent to a simple summation of the contributions from the two labeled components. This lack of any significant FRET is consistent with the monomeric nature of apoC-II under these conditions (Figs. 7 and 8). The addition of DHPS leads to a decrease in emission at 520 nm and an increase in emission at 617 nm, consistent with significant FRET resulting from lipid-induced oligomerization. The magnitude of this lipid-induced FRET signal, estimated from the increase in fluorescence emission at 617 nm, was similar for mixed samples at later time points, suggesting the presence of a stable oligomer. FRET was not observed in control experiments for the same mixture in the presence of denaturant (5 M GdnHCl).

The degree of FRET for mixtures of Alexa488-labeled apoC-II and Alexa594-labeled apoC-II was measured as a function of DHPS concentrations (Fig. 9). The results show that the FRET signal, measured either by an increase in intensity at 617 nm or as a decrease in intensity at 520 nm, increased systematically at submicellar DHPS concentrations and decreased at micellar DHPS concentrations. Fig. 9 also shows that the fluorescence intensity of Alexa488-labeled apoC-II alone at 520 nm varies with DHPS concentration in a manner that reflects the micellar state of DHPS (Fig. 2), whereas the fluorescence intensity of Alexa594-labeled apoC-II alone at 617 nm is essentially independent of DHPS concentration. Similar studies using DHPC showed that the FRET signals for mixtures of Alexa488-labeled apoC-II and Alexa594-labeled apoC-II were also dependent on lipid concentration, with submicellar DHPC (0–10 mM) inducing FRET and micellar DHPC (>10 mM) abolishing the FRET signal. These results are consistent with

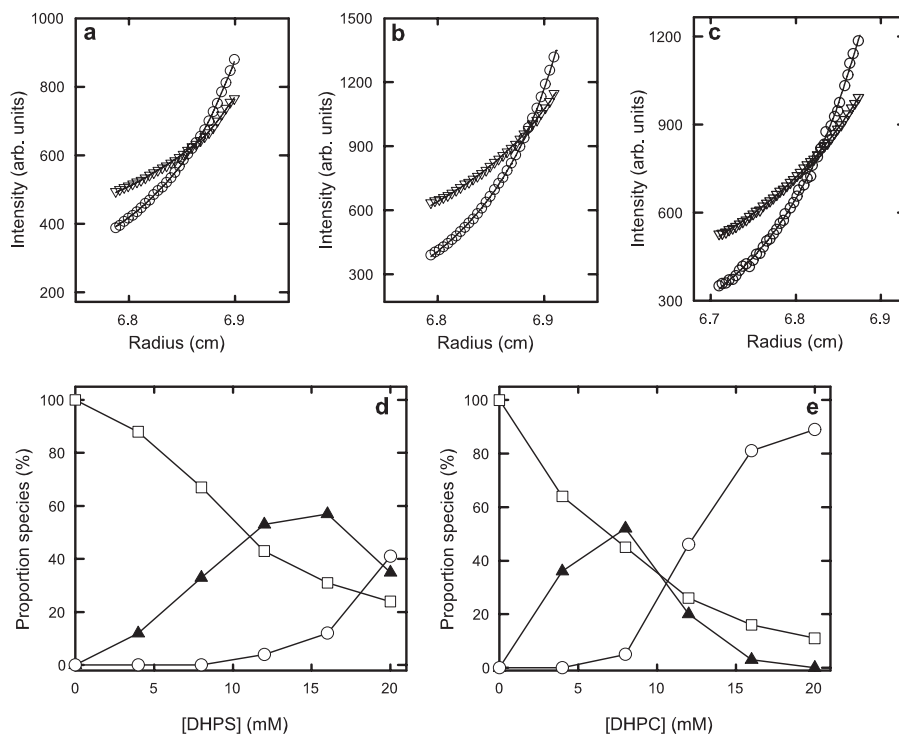


FIGURE 8. Sedimentation equilibrium analysis of Alexa488-labeled apoC-II in the presence of DHPC and DHPS. Representative sedimentation equilibrium distributions (detected by fluorescence intensity) are presented for apoC-II in aqueous buffers in the absence (a) and presence of 12 mM (b) and 20 mM (c) DHPS after centrifugation at 26,000 rpm ($54,500 \times g$) (open triangles) and 38,000 rpm ($116,000 \times g$), open circles. Data obtained at a range of DHPS concentrations in both H_2O and D_2O buffers were fitted to a three-species noninteracting model to obtain the partial specific volume and molecular weights of the species (Table 1). The proportions of each species were determined as a function of DHPS concentration (d). A similar set of experiments was conducted to obtain the proportions of Alexa488-labeled apoC-II species present as a function of DHPC concentration (e). Species 1 (open squares), species 2 (closed triangles), species 3 (open circles).

TABLE 1

Analysis of the effects of DHPC and DHPS on Alexa488-labeled apoC-II by sedimentation equilibrium and fluorescence detection in an analytical ultracentrifuge

Sedimentation equilibrium experiments on Alexa-labeled apoC-II (50 mg/ml) were performed at 20 °C using fluorescence detection. Equilibrium data were collected at angular velocities of 26,000 rpm ($54,500 \times g$) and 38,000 rpm ($116,000 \times g$) and in either H_2O - or D_2O -containing solutions for samples containing DHPS or DHPC. The data obtained for each phospholipid were analyzed globally using the program SEDPHAT (28), assuming three species to obtain best fit values for the buoyant molecular weights of the species in H_2O and D_2O . These values were used to calculate the partial specific volume (ν) and molecular weight (M) of the species (36). Estimates of the errors in the values were obtained using the Monte Carlo analysis from SEDPHAT.

Lipid present	Species	$M(1 - \nu\rho)_{\text{H}_2\text{O}}$	$M(1 - \nu\rho)_{\text{D}_2\text{O}}$	ν	M
DHPS ^a	1	2521 ± 21	1605 ± 26	0.730 ± 0.002	9560 ± 70
	2	10,717 ± 133	6594 ± 72	0.735 ± 0.003	40,700 ± 470
	3	4547 ± 52	1587 ± 31	0.826 ± 0.002	27,300 ± 330
DHPC ^a	1	2587 ± 19	1691	0.729 ± 0.002	9540 ± 60
	2	10,859 ± 133	6734 ± 52	0.734 ± 0.003	40,820 ± 520
	3	4982 ± 64	1728 ± 46	0.827 ± 0.002	28,800 ± 410

^a The concentrations of DHPS used were 0, 4, 8, 12, 16, and 20 μM . The concentrations of DHPC used were 0, 3, 6, 9, 12, and 15 μM . The apoC-II concentration was 50 $\mu\text{g}/\text{ml}$ in all cases.

Effects of Phospholipids on Amyloid Fibril Formation

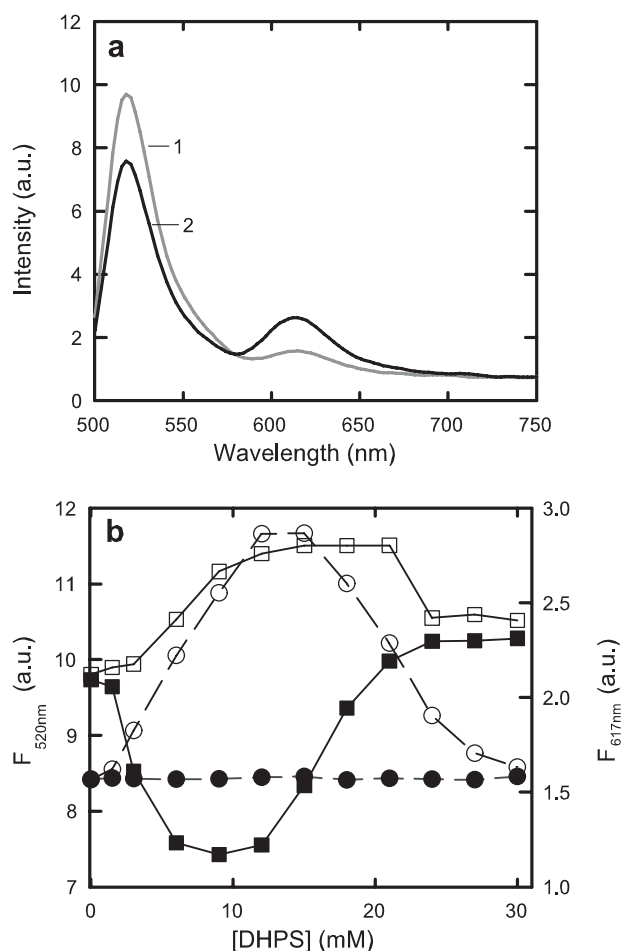


FIGURE 9. FRET analysis of DHPS-induced apoC-II tetramer formation. The excitation wavelength was 480 nm. *a*, fluorescence emission spectra of a mixture of Alexa594-labeled apoC-II (40 $\mu\text{g/ml}$) and Alexa488-labeled apoC-II (10 $\mu\text{g/ml}$) acquired 5 min after refolding in the absence of phospholipid (curve 1, gray line) and in the presence of 10 mM DHPS (curve 2, black line). *b*, effect of DHPS on the fluorescence emission intensity at 520 nm (closed squares) and 617 nm (closed circles) for a mixture of Alexa488-labeled apoC-II (10 $\mu\text{g/ml}$) and Alexa594-labeled apoC-II (40 $\mu\text{g/ml}$). Shown are control experiments for Alexa488-labeled apoC-II (10 $\mu\text{g/ml}$) alone (emission at 520 nm; open squares) and Alexa594-labeled apoC-II (40 $\mu\text{g/ml}$) alone (emission at 617 nm; open circles). *a.u.*, arbitrary fluorescence units.

the sedimentation analysis and indicate that the lipid-induced apoC-II tetramer is formed at an early stage in the refolding pathway.

Seeding of ApoC-II Fibril Formation—The increase in fluorescence emission of Alexa488-labeled apoC-II in the presence of submicellar lipid over the first 1–2 h (Figs. 4 and 5) indicated a slow process and provided an opportunity to determine whether the species formed during this phase can seed fibril formation. ApoC-II at 50 $\mu\text{g/ml}$ was preincubated with 10 mM DHPS for periods of 0–60 min and subsequently diluted into a freshly refolded apoC-II solution (0.2 mg/ml) to a final DHPS concentration of 500 μM . The results showed that preincubated samples systematically accelerate the rate of fibril formation by apoC-II compared with a control sample containing the same amount of DHPS but prepared without preincubation (Fig. 10). In contrast, preincubation of apoC-II (50 $\mu\text{g/ml}$) in the presence of micellar DHPS (20 mM) and subsequent dilution into a freshly refolded apoC-II solution (0.2 mg/ml) to a final DHPS

concentration of 500 μM did not alter the rate of fibril formation compared with the control (Fig. 10). These results support the hypothesis that the apoC-II tetramer formed in the presence of submicellar phospholipid during the early stages of refolding is an intermediate in the lipid activation pathway for apoC-II fibril formation.

DISCUSSION

Lipids and lipid metabolites present in amyloid deposits have the potential to affect several areas of amyloid metabolism, including the formation, stability, morphology, and toxicity of fibrils (5, 6, 8, 9, 18, 33). Most experimental studies have focused on lipid bilayers and membrane surfaces where many of the effects of lipids on fibril formation are variable, depending on the protein/lipid ratio and the degree of membrane penetration (34). However, a general observation of these studies is that amyloid fibril formation is favored by the presence of negatively charged lipid surfaces (5, 6, 34, 35). Lipids also affect protein folding and fibril formation at the level of individual lipid molecules. Monomeric lipids may arise through the oxidative cleavage of membrane lipids and the production of truncated derivatives, such as short chain phospholipids (7). Our previous studies on apoC-II showed that submicellar concentrations of short-chain phosphatidylcholine lipids increased the rate of fibril formation, whereas concentrated lipid micelles and bilayers completely inhibited this process (18). In view of the effect of negatively charged lipid surfaces on amyloid fibril formation, it was of interest to determine whether phospholipid charge might also affect the ability of submicellar and micellar lipids to modulate fibril formation. Our results show that DHPS and DHPC show a very similar activation profile for apoC-II fibril formation (Fig. 1), with the main difference attributable to the slightly higher CMC for DHPS compared with DHPC (Fig. 2). This suggests that the charged state of these phospholipid head groups has little effect and that the main factor causing accelerated fibril formation by submicellar lipids and inhibition by micellar lipids is an interaction with the hydrophobic fatty acyl chains. This is consistent with the observed correlation between the length of the fatty acid side chain and the effect on fibril growth (18).

Previous NMR and sedimentation studies of DHPC (30) showed that micelle formation occurs via a monomer-dimer-micelle equilibrium process, with dimer and micelle formation favored at higher concentrations. A similar micelle assembly pathway involving a DHPS dimer intermediate is also indicated (Fig. 2). The concentration dependence of dimer formation for both DHPC (30) and DHPS closely follows the profile for the activation of apoC-II fibril formation by these lipids, suggesting that phospholipid dimers may drive the initial steps in fibril assembly.

An unexpected finding in the present study was the difference between the time course of the fluorescence changes for Alexa-labeled apoC-II in the presence and absence of phospholipids. In the absence of phospholipid, the changes observed in both the fluorescence intensity and anisotropy correlated with fibril formation accompanied by a short lag phase. More complex kinetics were observed in the presence of submicellar DHPC and DHPS with three distinct phases observed. The first

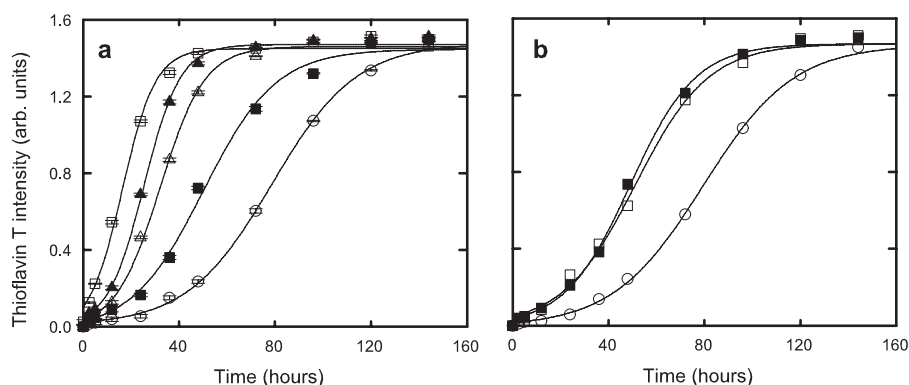


FIGURE 10. **Seeding of apoC-II fibril formation by preformed lipid-induced tetramer.** *a*, apoC-II (50 $\mu\text{g/ml}$) was incubated in the absence and presence of 10 mM DHPS for various times. Aliquots of these incubated solutions (100 μl) were then diluted into 1.9 ml of freshly diluted apoC-II to final concentrations of 0.2 mg/ml apoC-II and 500 μM DHPS in refolding buffer. The rate of fibril formation was monitored by ThT fluorescence. Results for samples preincubated with no DHPS (open circles) and with 10 mM DHPS for 15 min (open triangles), 30 min (closed triangles), and 60 min (open squares). A control sample containing 0.2 mg/ml apoC-II and 500 μM DHPS (closed squares) is included. *b*, as for *a*, except the concentration of DHPS in the preincubation mixture was 20 mM, and a single incubation time of 15 min was used with subsequent dilution of the sample to give final concentrations of 0.2 mg/ml apoC-II and 500 μM DHPS (closed squares). Results for a control sample containing 0.2 mg/ml apoC-II alone (open circles) and 0.2 mg/ml apoC-II in the presence of 500 μM DHPS (open squares) are included.

was a rapid increase in fluorescence intensity and anisotropy within the dead time of the measurements (<1 min). We attribute these changes to rapid lipid binding and self-association of apoC-II to form an oligomeric intermediate. This assertion is supported by the rapid changes in the FRET signal (within 5 min) observed for mixtures of Alexa488- and Alexa594-labeled apoC-II in the presence of submicellar DHPC and DHPS (Fig. 9). The second phase involved a slow increase in fluorescence intensity which was not accompanied by any significant change in fluorescence anisotropy. This suggests that this phase arises from a conformational change rather than a change in the state of aggregation. This conclusion is supported by the finding that the rate of change in the fluorescence intensity in this phase is independent of the initial starting concentration (Fig. 5). A possible explanation for this intermediate phase is a slow isomerization event, such as proline isomerization (37, 38), or domain interchange within the oligomer (39, 40). Alternatively, this phase may involve lipid rearrangement or lipid displacement from the oligomer. The third and slowest phase in Fig. 4 is a large decrease in fluorescence intensity accompanied by large increase in anisotropy. The magnitudes of these changes are similar to those observed in the absence of lipid and are consistent with the gradual formation of amyloid fibrils. The rate of this last phase is dependent on apoC-II concentrations, as expected for apoC-II fibril growth (23). The final phase was not present at low apoC-II concentration (50 $\mu\text{g/ml}$), consistent with the finding that apoC-II fibrils do not form at this concentration.

The availability of a sensitive and specific fluorescence detection system for the analytical ultracentrifuge provided an opportunity to characterize the state of association of apoC-II oligomers at low concentrations in the absence of fibril formation. This technology has the potential to characterize oligomeric amyloid precursors at concentrations that have hitherto been inaccessible and under conditions where fibril formation is negligible. Sedimentation velocity experiments over a range

of Alexa-labeled apoC-II concentrations (5–50 $\mu\text{g/ml}$) in the absence of lipids indicated a single monomeric species (results not shown), suggesting that oligomeric species do not accumulate under these conditions. In contrast, in the presence of DHPC and DHPS, two additional species appear (Fig. 7). Sedimentation equilibrium analysis established these species as an apoC-II tetramer formed at submicellar phospholipid concentrations and an apoC-II-micelle complex at higher lipid concentrations. Comparison of the lipid concentration dependence of tetramer formation with the changes in secondary structure (Fig. 3) indicates that the apoC-II tetramer has increased β -structure compared with the apoC-II monomer and the apoC-II-micelle complex.

Furthermore, the results of seeding experiments (Fig. 10) indicate that the apoC-II tetrameric intermediate seeds apoC-II fibril formation, suggesting that the tetramer is on the pathway to fibril formation. Characterization of this tetrameric intermediate using FRET provides a simple spectroscopic signal that could be useful for high throughput screening of amyloid fibril inhibitors. The ability to identify a discrete tetrameric intermediate offers the prospect of more detailed structural analysis of this oligomeric species and the way it participates in the self-assembly, metabolism, and toxicity of amyloid fibrils.

Acknowledgments—We are greatly indebted to Dr. Chi L. L. Pham and Lynne Waddington for assistance with electron microscopy.

REFERENCES

- Sipe, J. D., and Cohen, A. S. (2000) *J. Struct. Biol.* **130**, 88–98
- Alexandrescu, A. T. (2005) *Protein Sci.* **14**, 1–12
- Terzi, E., Holzemann, G., and Seelig, J. (1997) *Biochemistry* **36**, 14845–14852
- Lee, H. J., Choi, C., and Lee, S. J. (2002) *J. Biol. Chem.* **277**, 671–678
- Knight, J. D., and Miranker, A. D. (2004) *J. Mol. Biol.* **341**, 1175–1187
- Zhao, H., Tuominen, E. K., and Kinnunen, P. K. (2004) *Biochemistry* **43**, 10302–10307
- Schlame, M., Haupt, R., Wiswedel, I., Kox, W. J., and Rustow, B. (1996) *J. Lipid Res.* **37**, 2608–2615
- Zhang, Q., Powers, E. T., Nieva, J., Huff, M. E., Dendle, M. A., Bieschke, J., Glabe, C. G., Eschenmoser, A., Wentworth, P., Jr., Lerner, R. A., and Kelly, J. W. (2004) *Proc. Natl. Acad. Sci. U. S. A.* **101**, 4752–4757
- Bosco, D. A., Fowler, D. M., Zhang, Q., Nieva, J., Powers, E. T., Wentworth, P., Jr., Lerner, R. A., and Kelly, J. W. (2006) *Nat. Chem. Biol.* **2**, 249–253
- Stewart, C. R., Wilson, L. M., Zhang, Q., Pham, C. L., Waddington, L. J., Staples, M. K., Stapleton, D., Kelly, J. W., and Howlett, G. J. (2007) *Biochemistry* **46**, 5552–5561
- Hatters, D. M., and Howlett, G. J. (2002) *Eur. Biophys. J.* **31**, 2–8
- Hatters, D. M., MacPhee, C. E., Lawrence, L. J., Sawyer, W. H., and Howlett, G. J. (2000) *Biochemistry* **39**, 8276–8283
- Stewart, C. R., Haw, A., Lopez, R., McDonald, T. O., Callaghan, J. M., McConville, M. J., Moore, K. J., Howlett, G. J., and O'Brien, K. D. (2007) *J. Lipid Res.* **48**, 2162–2171

Effects of Phospholipids on Amyloid Fibril Formation

14. Medeiros, L. A., Khan, T., El Khoury, J. B., Pham, C. L., Hatters, D. M., Howlett, G. J., Lopez, R., O'Brien, K. D., and Moore, K. J. (2004) *J. Biol. Chem.* **279**, 10643–10648
15. Moore, K. J., El Khoury, J., Medeiros, L. A., Terada, K., Geula, C., Luster, A. D., and Freeman, M. W. (2002) *J. Biol. Chem.* **277**, 47373–47379
16. MacRaild, C. A., Hatters, D. M., Howlett, G. J., and Gooley, P. R. (2001) *Biochemistry* **40**, 5414–5421
17. MacRaild, C. A., Howlett, G. J., and Gooley, P. R. (2004) *Biochemistry* **43**, 8084–8093
18. Griffin, M. D., Mok, M. L., Wilson, L. M., Pham, C. L., Waddington, L. J., Perugini, M. A., and Howlett, G. J. (2008) *J. Mol. Biol.* **375**, 240–256
19. Hatters, D. M., Lawrence, L. J., and Howlett, G. J. (2001) *FEBS Lett.* **494**, 220–224
20. Kirkitadze, M. D., Bitan, G., and Teplow, D. B. (2002) *J. Neurosci. Res.* **69**, 567–577
21. Walsh, D. M., Klyubin, I., Fadeeva, J. V., Cullen, W. K., Anwyl, R., Wolfe, M. S., Rowan, M. J., and Selkoe, D. J. (2002) *Nature* **416**, 535–539
22. Kaye, R., Head, E., Thompson, J. L., McIntire, T. M., Milton, S. C., Cotman, C. W., and Glabe, C. G. (2003) *Science* **300**, 486–489
23. Binger, K. J., Pham, C. L., Wilson, L. M., Bailey, M. F., Lawrence, L. J., Schuck, P., and Howlett, G. J. (2008) *J. Mol. Biol.* **376**, 1116–1129
24. MacGregor, I. K., Anderson, A. L., and Laue, T. M. (2004) *Biophys. Chem.* **108**, 165–185
25. Edwards, K., Chan, R. Y., and Sawyer, W. H. (1994) *Biochemistry* **33**, 13304–13311
26. Sreerama, N., and Woody, R. W. (2000) *Anal. Biochem.* **287**, 252–260
27. Schuck, P. (2003) *Anal. Biochem.* **320**, 104–124
28. Vistica, J., Dam, J., Balbo, A., Yikilmaz, E., Mariuzza, R. A., Rouault, T. A., and Schuck, P. (2004) *Anal. Biochem.* **326**, 234–256
29. Hatters, D. M., Minton, A. P., and Howlett, G. J. (2002) *J. Biol. Chem.* **277**, 7824–7830
30. Atcliffe, B. W., MacRaild, C. A., Gooley, P. R., and Howlett, G. J. (2001) *Eur. J. Biochem.* **268**, 2838–2846
31. Tausk, R. J., Karmiggelt, J., Oudshoorn, C., and Overbeek, J. T. (1974) *Biophys. Chem.* **1**, 175–183
32. Johnson, R. E., Wells, M. A., and Rupley, J. A. (1981) *Biochemistry* **20**, 4239–4242
33. Myers, S. L., Jones, S., Jahn, T. R., Morten, I. J., Tennent, G. A., Hewitt, E. W., and Radford, S. E. (2006) *Biochemistry* **45**, 2311–2321
34. Bokvist, M., Lindstrom, F., Watts, A., and Grobner, G. (2004) *J. Mol. Biol.* **335**, 1039–1049
35. Olofsson, A., Borowik, T., Grobner, G., and Sauer-Eriksson, A. E. (2007) *J. Mol. Biol.* **374**, 186–194
36. Edelstein, S. J., and Schachman, H. K. (1973) *Methods Enzymol.* **27**, 82–98
37. Eakin, C. M., Berman, A. J., and Miranker, A. D. (2006) *Nat. Struct. Mol. Biol.* **13**, 202–208
38. Jenko Kokalj, S., Guncar, G., Stern, I., Morgan, G., Rabzelj, S., Kenig, M., Staniforth, R. A., Waltho, J. P., Zerovnik, E., and Turk, D. (2007) *J. Mol. Biol.* **366**, 1569–1579
39. Liu, Y., and Eisenberg, D. (2002) *Protein Sci.* **11**, 1285–1299
40. Sanders, A., Jeremy Craven, C., Higgins, L. D., Giannini, S., Conroy, M. J., Hounslow, A. M., Waltho, J. P., and Staniforth, R. A. (2004) *J. Mol. Biol.* **336**, 165–178
41. Schuck, P., and Rossmann, P. (2000) *Biopolymers* **54**, 328–341